Optimization of the Prompt Fission Neutron Spectra of ^{239}Pu(n, f) via Criticality Benchmarking*

Jia-hao Chen,[1] Bo Yang,[1,†] Qing-gang Jia,[1] Rui Li,[2] Wen-di Chen,[1] Hai-rui Guo,[1] Wei-li Sun,[1] and Tao Ye[1,‡]

[1]*Institute of Applied Physics and Computational Mathematics, Beijing 100094, China*
[2]*CAEP Software Centre for High Performance Numerical Simulation (CAEP-SCNS), Beijing 100088, China*

Prompt fission neutron spectra (PFNS) play a significant role in nuclear science and technology. In this work, we report on the evaluation of the PFNS for ^{239}Pu through both differential and integral experimental data. We introduce a method that leverages integral criticality benchmark experiments to constrain the PFNS data. By constructing a covariance matrix, we perturbed the measured central values of the PFNS. The PFNS were sampled using two types of covariance matrices. One was generated with an assumed correlation matrix and incorporating experimental uncertainties, and the other was derived directly from experiment reports. The Joint Monte Carlo Transport (JMCT) code was employed to perform transport simulations on five criticality benchmark assemblies, utilizing the perturbed PFNS data. The extensive simulations resulted in an optimized PFNS that showed improved agreement with integral criticality benchmark experiments. This study introduces a novel approach for optimizing differential experimental data through integral experiments, especially when a covariance matrix is not provided.

Keywords: Prompt fission neutron spectra, Differential nuclear data, Criticality benchmark, Random sample, Transport simulation

I. INTRODUCTION

Nuclear fission has been widely applied in the nuclear engineering, due to the substantial energy release during the process. Despite the existence of many models that aid in understanding the mechanism of nuclear fission [1–6], the current understanding of the actual processes occurring in nuclear fission remain incomplete, both in terms of experimental observations and theoretical research [7–10]. Nuclear data serves as the fundamental basis for understanding the physical mechanisms of nuclear fission and its diverse applications in nuclear engineering. As an important fission nucleus, ^{239}Pu is widely used in accelerator-driven subcritical systems and fast neutron reactors [11, 12]. So the nuclear data of neutron-induced fission of ^{239}Pu has received extensive attention. Specifically, the prompt fission neutron spectra (PFNS) of neutron-induced ^{239}Pu fission exhibit significant applications in reactor calculations, shielding, nuclear fuel management and the transmuting nuclear wastes. This has naturally inspired continuous interests in enhancing the accuracy of PFNS for these applications [13, 14].

Measuring Prompt Fission Neutron Spectra (PFNS) is a crucial task in nuclear physics, commonly achieved through the use of a fission chamber combined with the neutron time-of-flight (TOF) technique. This method obtains the energy of fission neutrons by measuring the time difference between the time signals generated by the fission fragments and the time signals of the emitted neutrons [15]. With the development of experimental detection techniques, several experiments have measured different energy regions of the PFNS of ^{239}Pu(n, f) with various incident neutron energies [16–20]. However, experimental data often suffer from low statistics and complex analyses, which can result in incomplete coverage of all energy domains, large uncertainties, and inconsistencies [16–20].

In practice, the evaluated data are used in various engineering applications. The evaluation process often involves both experimental data and theoretical calculations. Typical models, such as the Maxwellian distribution, Watt spectrum, and Los Alamos Model [21–23], are often used for evaluation, aiming to provide the evaluated data across the whole energy range. However, it is important to note that the current state of PFNS within evaluated nuclear data libraries is not yet fully satisfactory. Despite the existence of several international libraries such as CENDL-3.2 [24], ENDF/B-VIII.0 [25], JENDL-5 [26], JEFF-3.3 [27] and others, inconsistencies in PFNS remain. This underscores the need for further research to enhance the accuracy and consistency of the data.

The uncertainty in differential experimental data is often relatively large. Due to the use of similar detection methods in most experiments, this can lead to some unidentified biases or errors, resulting in wrong evaluation of mean values and covariances [28]. Given that the measurement accuracy of physical quantities in integral experiments is often higher and directly related to practical applications, it can be considered to use integral experimental data to constrain differential experimental data. Currently, there are studies that aim to provide guidance for improving evaluation data through integral experiments. These methods typically constrain microscopic data by simulating integral experiments, employing models to represent the microscopic data and utilizing sensitivity analysis and Bayesian methods to adjust the microscopic data [28–31].

However, the uncertainties derived from the propagation of model parameter uncertainties in PFNS models tend to be smaller at certain outgoing energies, and this is often not consistent with the uncertainties typically observed in experimental PFNS. Furthermore, the uncertainties attributable to the model's inherent shortcomings are usually not estimated and

* This work was supported by the National Natural Science Foundation of China (No.12347126)
† Corresponding author, yang_bo@iapcm.ac.cn
‡ Corresponding author, ye_tao@iapcm.ac.cn

not included in the evaluation process [32–34]. In order to both minimize the impact of the model on data optimization and circumvent the sensitivity analysis requirement that the integral quantity must exhibit a linear response to the differential quantity, we perturb the latest differential experimental data to generate a significant amount of PFNS data. Subsequently, these perturbed PFNS are then incorporated as input into the transport simulation. By comparing the calculated integral quantity k_{eff} for the criticality benchmarks, we evaluate the quality of the perturbed PFNS.

Generally, we can perform the perturbation based on the covariance matrix. However, the covariance matrix in experiments typically needs to be obtained through sufficient experimental information, such as counting statistics, background correction, detector efficiency determination, finite time resolution, an uncertainty in the TOF length, etc. [35]. Furthermore, many experimentalists do not report this information clearly enough, especially in some early experiments.

Therefore, in the present work, we utilized an assumed correlation matrix combined with experimental uncertainties to generate a covariance matrix. Additionally, we conducted sampling using the covariance matrix provided by the experiment for comparative analysis. This approach offers a novel idea for optimizing microscopic experimental data through integral experiments. Specifically, this method can be applied to the optimization of microscopic experimental data when a covariance matrix is not provided.

II. METHODS

Considering the relatively large uncertainties associated with differential experiments, and taking into account the higher precision of integral experimental data, as well as the fact that criticality benchmark experiments have already been employed for validating and improving nuclear data[36, 37], alongside their similarity to engineering applications, we aim to maximize the utilization of the existing experimental data. To achieve this, we employ the integral nuclear data k_{eff} as the target quantity to constrain the microscopic nuclear data, specifically the prompt fission neutron spectra (PFNS) of ^{239}Pu. The main idea is to use the differential experimental data and its associated uncertainty information to perturb the experimental values, and then utilize these perturbed data in transport simulations to determine the optimal differential data.

To minimize the impact of models on this method, we adopt a data-driven approach to constrain the prompt fission neutron spectra (PFNS). As the Watt-Maxwellian function has four adjustable parameters, it exhibits flexibility in describing PFNS [32, 38]. Consequently, experimental data are typically well-fitted by the Watt-Maxwellian function. We exclusively employ the Watt-Maxwellian function to describe the differential data, leveraging its properties of normalization and non-negativity to ensure that the PFNS maintains the characteristics of shape spectra and also to enable extrapolation of differential data beyond the available range. The Watt-Maxwellian function is a linear combination of a Maxwellian and a Watt distribution as:

$$
\begin{aligned}
f_{WM}(E) &= w_M f_M\left(E, E_M\right) + \left(1 - w_M\right) f_W\left(E, a_W, b_W\right) \\
f_M\left(E, E_M\right) &= K_M \sqrt{E} e^{-E/E_M} \\
f_W\left(E, a_W, b_W\right) &= K_W e^{-E/a_W} \sinh \sqrt{b_W E}
\end{aligned}
\tag{1}
$$

where w_M is the weight of the Maxwellian function, w_M, E_M, a, b are all adjustable parameters that can be used for fitting the function. By fitting the differential experimental data, we can obtain the PFNS in the form of Watt-Maxwellian under different incident energies.

A. Generation of perturbed PFNS

The differential experimental data used in this method is sourced from the EXFOR database and is reported in the Refs. [39, 40] by Kelly *et al*. These references report the latest experimental data on neutron-induced prompt fission neutron spectra (PFNS) of ^{239}Pu, covering 20 average incident energy points ranging from 1 to 20 MeV. Compared with the measurement results in previous literature, this dataset has achieved breakthroughs in terms of accuracy, detailed uncertainty analysis, and thorough investigations of necessary corrections [39, 41].

By utilizing the experimental uncertainty information, we proposed to perturb the data around the experimental measurements to generate perturbed PFNS for the transport code simulations. However, due to the large number of data points, a gridded approach for generating points, where candidate values are generated at each energy point based on the mean values and error bars, would significantly slow down the calculation process as the computational load grows exponentially with the number of data points. To reduce the computational cost, this work introduces a sampling method that utilizes a covariance matrix to reduce the dimensionality of data variations. This enables us to obtain relatively optimized PFNS with fewer simulation calculations, thereby improving computational efficiency.

The experimental nuclear reaction database EXFOR often includes experimental data accompanied by uncertainties, but covariance data is not always provided. To pursue a method applicable to general scenarios, particularly when confronted with the absence of a reported covariance matrix, we have constructed the correlation matrix based on certain characteristics observed in the correlation matrix provided in Ref. [39, 40], and generate the covariance matrix by combining the uncertainty information from the experiments. The correlation matrix diagram in Ref. [39, 40] shows an extremely high correlation between PFNS at different neutron incident energies. Therefore, assuming that the correlation between different data points in the PFNS spectrum decreases exponentially with the square of their distance, as shown in Eq. 2, we can construct a covariance matrix based on this assumption and use it to perturb each data point of the PFNS spectrum at a single incident energy.

$$\mathrm{cor}_{ij} = e^{-\frac{d_{ij}^2}{2\sigma^2}} \qquad (2)$$
$$d_{ij} = |i - diag_j|$$

where $diag_j$ represents the diagonal element coordinate in the jth row and i denotes the position of the ith element within the same jth row. The value of σ indicates the rate at which the correlation decreases as the distance increases. This assumption can capture some of the patterns in the experimental data and effectively reduce the degrees of freedom for data perturbation.

To mitigate the impact of excessive uncertainty at low energy points on the fitting function, we select data points within the energy range consistent with the diagrams reported in the literature, specifically choosing points greater than 100 keV for outgoing neutron energies. Based on the above description, we use the total uncertainty as the standard deviation, which is the square root of the variance. To obtain the covariance matrix, we rely on the definition of correlation provided in Eq. 3 [42]. From this definition, it is straightforward to derive Eq. 4. By combining this derived equation with the assumed correlation matrix, we are able to compute the covariance matrix.

$$\mathrm{cor}_{ij} = \frac{\mathrm{cov}_{ij}}{\sqrt{\mathrm{cov}_{ii}\mathrm{cov}_{jj}}} \qquad (3)$$
$$\mathrm{var}_i = \mathrm{cov}_{ii}$$

$$\mathrm{cov}_{ij} = \mathrm{cor}_{ij}\sqrt{\mathrm{cov}_{ii}\mathrm{cov}_{jj}} \qquad (4)$$

where the var denotes the variance vector, cor_{ij} represents the element in the ith column and jth row of the correlation matrix, and cov_{ij} represents the element in the ith column and jth row of the covariance matrix. Using the generated covariance matrix, we can perturb the differential experimental data, thereby producing PFNS discrete points near the differential experimental data. Since the new PFNS is obtained through sampling, it does not inherently possess the properties of a shape spectrum. To address this, we employ the Watt-Maxwellian function to fit the perturbed data in order to generate a continuous, normalized, and non-negative PFNS. The fitting results are illustrated in Fig. 1.

As depicted in Fig. 1, random sampling utilizing the covariance matrix effectively generates perturbed data proximal to the experimental data, and the Watt-Maxwellian function exhibits a robust fit to these perturbed data points. For a comprehensive set of PFNS encompassing various incident energies, a strong correlation across PFNS at different incident energies can be achieved by selecting a uniform random number seed. This novel sampling and fitting methodology yields a substantial quantity of continuous PFNS.

B. Using the perturbed data for transport calculations.

To correlate differential data with integral data, we can employ transport calculations, using differential data as input and generating integral data as output, which can then be compared with the benchmarks. In this study, the Joint Monte Carlo Transport (JMCT) code was utilized to perform criticality computations. [43–45] To optimize the PFNS, during transport calculations, except for the PFNS data, all other nuclear data were obtained from the ENDF/B-VIII.0 library [25]. To generate PFNS data suitable for utilization in this code, we employ the Nuclear Data Processing System (NJOY2016) to process the perturbed PFNS data, transforming it into ACE format [46]. To facilitate subsequent comparisons with the results from ENDF/B-VIII.0, we adopt the same incident energy selections as those in ENDF/B-VIII.0. Since the experimental data do not perfectly align with this set of incident energies, we employ linear interpolation to generate PFNS for various incident energies. As the range of experimental incident energies is slightly narrower than that of ENDF/B-VIII.0, we opt to extrapolate PFNS for energies below the minimum experimental average incident energy of 1.54 MeV or above the maximum experimental incident energy of 19.59 MeV in ENDF/B-VIII.0. Specifically, we utilize a consistent approach of linear extrapolation, analogous

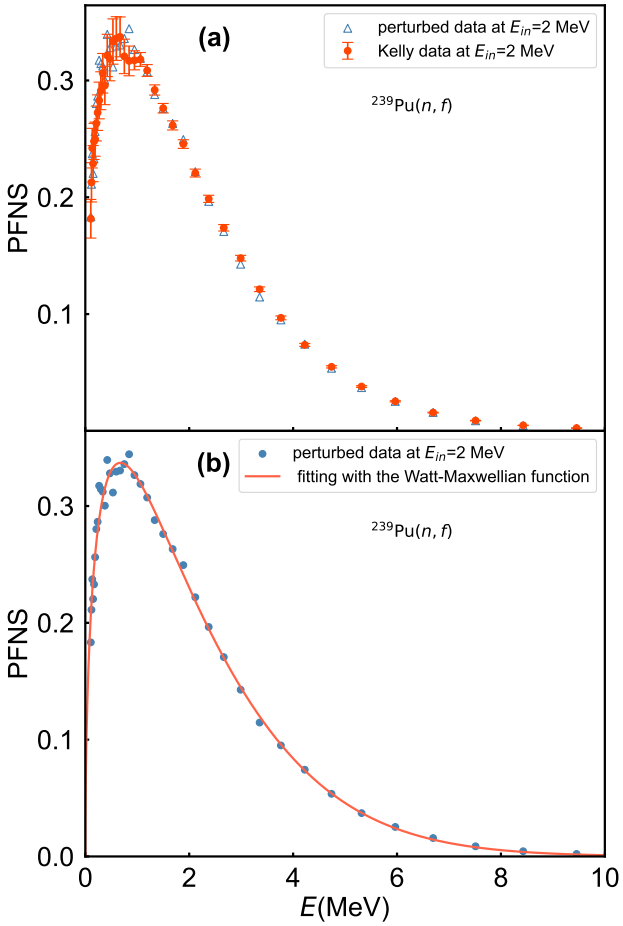

Fig. 1. (Color Online) Prompt fission neutron spectra (PFNS) of ^{239}Pu(n, f) for (a) perturbed data, shown by blue hollow triangles, in comparison to literature values shown by red points[39], and (b) perturbed data, shown by blue points, along with the fitting result to the data.

to the aforementioned linear interpolation method, to predict PFNS at these incident energies.

Given that the differential experimental data employed in this study is limited to an incident energy range above 1 MeV, the selection of fast neutron spectra becomes the more appropriate choice for this specific energy domain. To minimize the possible uncertainty in the transport process while also covering as much of the experimental data region as possible, we have selected five criticality benchmarks with relatively straightforward geometric configurations. Each of these benchmarks is characterized by a dominant "FAST" flux spectrum and is directly associated with the nuclide ^{239}Pu. The specific benchmark cases employed in this study are Pu-Met-Fast-002, Pu-Met-Fast-003, Pu-Met-Fast-008, Pu-Met-Fast-009, and Pu-Met-Fast-010 [47, 48]. In the benchmarks utilized above, Pu-Met-Fast-002 denotes a bare experiment (20.1 at.% ^{240}Pu). Pu-Met-Fast-003 represents an array of plutonium metal buttons in an unmoderated configuration. Pu-Met-Fast-008 signifies an experiment involving a thorium reflector. Pu-Met-Fast-009 represents an aluminum reflected experiment. Lastly, Pu-Met-Fast-010 denotes an experiment utilizing a natural uranium reflector [49]. By utilizing these relatively straightforward criticality benchmark assemblies , which encompass a diversity of configurations, we aim to enhance the robustness of constraints on differential data through the integration of experimental data. The input for JMCT uses CAD modeling [45], and the models of these criticality benchmarks are constructed based on information sourced from the MIT Computational Reactor Physics Group [50].

All cases were executed using the same perturbed data, each simulation using 10000 neutrons per cycle, with 100 inactive cycles and 1400 additional active cycle. The uncertainty of the calculated eigenvalue $k_{\rm eff}$ exhibits a slight variability depending on the device and input files, yet it consistently remains below 20 pcm. This value is notably smaller in comparison to the benchmark uncertainties.

C. Calculated $\delta k_{\rm eff}$

To evaluate the quality of each perturbed prompt fission neutron spectra (PFNS), we conduct a comparative analysis between the eigenvalue $k_{\rm eff}$ derived from transport simulations for five criticality benchmarks and their respective benchmark values. Specifically, we employ the relative calculation-to-experimental ratio, denoted as $\frac{|\mathrm{C-E}|}{\mathrm{E}}$, to quantitatively assess the deviation between the calculated $k_{\rm eff}$ and the benchmark $k_{\rm eff}$ values, which are sourced from Ref. [47]. Notably, the benchmark $k_{\rm eff}$ values for these benchmark integration experiments are all 1.000. The relative difference between the calculated and experimental values is defined by Eq.5, where $k^{\rm cal}_{\rm eff,b}$ represents the calculated $k_{\rm eff}$ for the b-th criticality benchmark assembly, and $k^{\rm ben}_{\rm eff,b}$ represents the benchmark value of $k_{\rm eff}$ for the same assembly. Furthermore, we introduce the total relative difference, denoted as $\delta k^{\rm tot}_{\rm eff}$, which is defined as the average of $\delta k_{\rm eff,b}$ calculated for all criticality benchmarks, as outlined in Eq.6, This approach enables us to identify the most suitable perturbed PFNS that best captures the integral experimental behavior and achieves optimal results.

$$\delta k_{\rm eff,b} = \frac{|k^{\rm cal}_{\rm eff,b} - k^{\rm ben}_{\rm eff,b}|}{k^{\rm ben}_{\rm eff,b}} \tag{5}$$

$$\delta k^{\rm tot}_{\rm eff} = \frac{\sum_b \delta k_{\rm eff,b}}{5} \tag{6}$$

To provide clarity on the entire process of utilizing integral experimental data to constrain differential experimental data, we have created a flowchart for the aforementioned method, which is presented in Fig. 2. By sampling from the covariance matrix, we obtain perturbed prompt fission neutron spectra (PFNS) that are distributed near the differential experimental data. These perturbed PFNS are then processed using the NJOY code to generate data in ACE format. For each set of perturbed PFNS, the JMCT is employed to perform transport simulations on five criticality benchmarks. Through extensive simulations, we are able to identify the perturbed PFNS that not only exhibit the closest alignment with the benchmark values but also maintain a close proximity to the original differential experimental data. This approach ensures a robust and reliable method for constraining differential experimental data using integral experimental information, ultimately enhancing the accuracy and applicability the differential experimental data.

III. RESULTS AND DISCUSSION

A. Calculation results from generated covariance matrix

Following the steps in Fig. 2, initially, we generate the covariance matrix based on Eq. 2, with the assumption that $\sigma = 1$. This assumption allows us to derive a correlation matrix that exhibits a relatively rapid decrease in correlation between data points. By incorporating the uncertainty data provided in the experiment [40], we can obtain the covariance matrix for this specific scenario. Subsequently, we employ this covariance matrix to perform random sampling of data points, generating perturbed datasets. In this framework, we executed 1,000 samplings and calculated the corresponding $\delta k^{\rm tot}_{\rm eff}$ for each sampling. This process ultimately yields the distribution of $\delta k^{\rm tot}_{\rm eff}$, as presented in Fig. 3.

Fig. 3 (a) illustrates the impact of PFNS sampled from generated covariance data on transport calculations. The scattered random distribution of the points in the figure reflecting the stochastic nature of the sampling process. It is evident that different PFNS lead to variations in the computed $k_{\rm eff}$ values, demonstrating that adjustments to differential data within the error bands can have an effect on integral data. This further validates the effectiveness of constraining differential experiments through integral experiments. Fig. 3 (b) displays a histogram of the statistical distribution of $\delta k^{\rm tot}_{\rm eff}$, revealing a

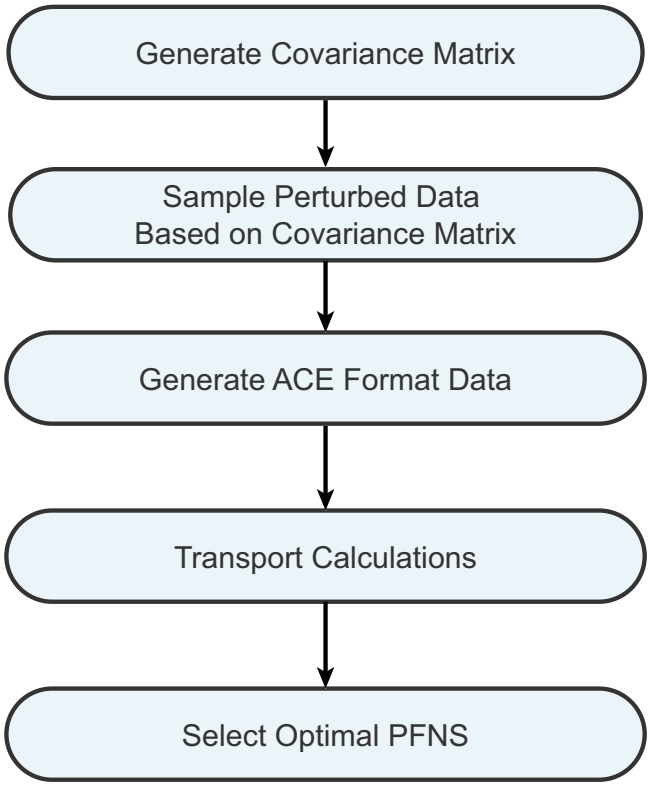

Fig. 2. Flowchart of optimizing the differential PFNS process through the use of integration experiments

rapid decrease at both ends of the distribution. The red Gaussian function fit line in Fig. 3 (b) also shows that as $\delta k_{\mathrm{eff}}^{\mathrm{tot}}$ becomes smaller, its statistical distribution exhibits an exponential decay. This suggests that the current sampling, with σ = 1.0, is statistically sufficient for obtaining the optimal value. Additionally, Fig. 3 (b) shows that optimizing the calculation of k_{eff} by adjusting only the PFNS method ultimately leads to an optimal value of $\delta k_{\mathrm{eff}}^{\mathrm{tot}}$ near 0.002. The optimal PFNS obtained through our sampling corresponds to a $\delta k_{\mathrm{eff}}^{\mathrm{tot}}$ value of 0.00219. When calculations are performed using the ENDF/B-VIII.0 library, the resulting $\delta k_{\mathrm{eff}}^{\mathrm{tot}}$ value is 0.00299. This comparison indicates that our PFNS, perturbed using the latest experimental data, performs better in integral experimental validation compared to the PFNS in the ENDF/B-VIII.0 library.

To broaden the scope for parameter variation, we have chosen different values for σ in Eq. 2. By choosing distinct σ values, we alter the rate of decrease in correlation for the correlation matrix, thereby generating different covariance matrices. Additionally, we have selected σ = 0.1, 0.2, 0.5, 1.5, 2.0, and 5.0, and employed the method detailed in Section II to generate covariance matrices. Analogous to the case where σ = 1.0, we can compute $\delta k_{\mathrm{eff}}^{\mathrm{tot}}$ for a range of σ values. Owing to the variations in the covariance matrix, the distribution of the computed $\delta k_{\mathrm{eff}}^{\mathrm{tot}}$ will also exhibit differences. For each value of σ, 1000 samples were taken, and the $\delta k_{\mathrm{eff}}^{\mathrm{tot}}$ calculated based on the perturbed PFNS generated by the sampling is shown in Fig. 4.

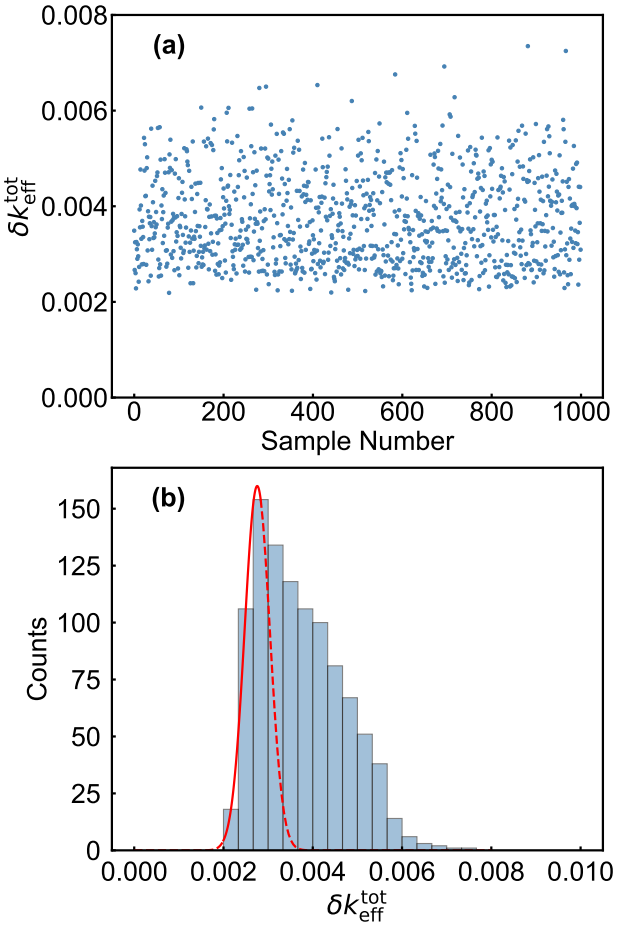

Fig. 3. (Color Online) Assuming σ = 1.0, the distribution of $\delta k_{\mathrm{eff}}^{\mathrm{tot}}$ obtained by comparing the transport calculated results with the benchmark values through is shown as follows: (a) a two-dimensional plot of $\delta k_{\mathrm{eff}}^{\mathrm{tot}}$ versus sample number; (b) a histogram of the statistical distribution of $\delta k_{\mathrm{eff}}^{\mathrm{tot}}$. The red line represents a Gaussian function fit to the histogram in the range of $\delta k_{\mathrm{eff}}^{\mathrm{tot}}$ = 0.002 to 0.003, with the red solid line indicates the fitting range.

As can be observed from Fig. 4, although the distribution of $\delta k_{\mathrm{eff}}^{\mathrm{tot}}$ varies under different σ values, its main characteristic remains consistent: the distribution of $\delta k_{\mathrm{eff}}^{\mathrm{tot}}$ decreases rapidly at both ends. Notably, at the left end of the horizontal axis in Fig. 4, all cases exhibit the same characteristic as when σ = 1.0, that is, as the value of $\delta k_{\mathrm{eff}}^{\mathrm{tot}}$ on the x axis of Fig. 4 decreases, its statistics drop exponentially, converging near 0.002. This indicates that the results obtained using a sample size of 1000 are sufficient to generally represent the distribution of $\delta k_{\mathrm{eff}}^{\mathrm{tot}}$. Although it is acknowledged that a larger sample size would yield results closer to the optimal value when using sampling methods to obtain the best PFNS, the current sample size has already provided a satisfactory approximation.

So far, we have obtained the perturbed PFNS under seven distinct σ values. We can now compile all of these results together, allowing us to utilize the statistical information from the entire sampling process. The overall distribution of $\delta k_{\mathrm{eff}}^{\mathrm{tot}}$

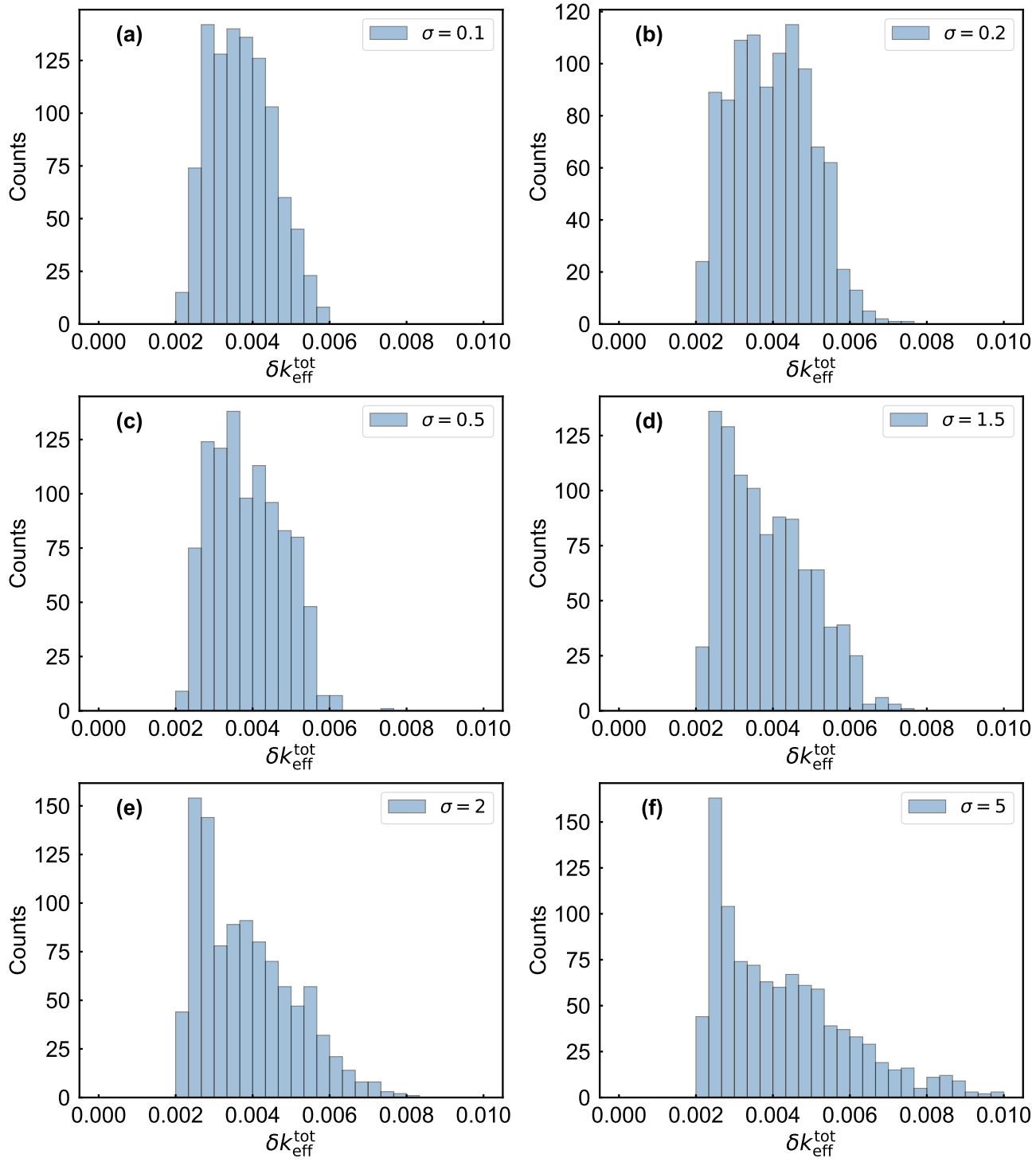

Fig. 4. The distribution of $\delta k_{\mathrm{eff}}^{\mathrm{tot}}$ obtained by comparing the transport calculated results with the benchmark values under the following case: (a) σ = 0.1; (b) σ = 0.2; (c) σ = 0.5; (d) σ = 1.5; (e) σ = 2.0; (f) σ = 5.0.

obtained from all sampling results is shown in Fig. 5. In the cases of various σ values mentioned earlier, the distribution of $\delta k_{\mathrm{eff}}^{\mathrm{tot}}$ decreases rapidly at both ends, especially showing an exponential decrease trend at the low $\delta k_{\mathrm{eff}}^{\mathrm{tot}}$ end and converges near 0.002. As a synthesis of the previous data, Fig. 5 naturally exhibits such characteristics in the distribution of $\delta k_{\mathrm{eff}}^{\mathrm{tot}}$. However, due to the improvement in statistics and the superposition of various σ cases, the statistical fluctuations of the distribution decrease, resulting in a more continuous distribution. The optimal $\delta k_{\mathrm{eff}}^{\mathrm{tot}}$ obtained for all the perturbed

PFNS generated through the method based on covariance matrix creation and sampling is 0.00210. This value is very close to the optimal $\delta k_{\rm eff}^{\rm tot}$ previously obtained by considering only the case where σ = 1.0, which also indicates the rapid decrease of $\delta k_{\rm eff}^{\rm tot}$ at the low $\delta k_{\rm eff}^{\rm tot}$ end.

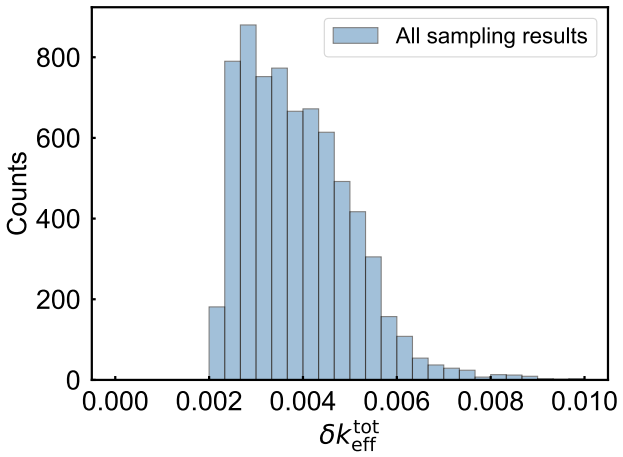

Fig. 5. The distribution of $\delta k_{\rm eff}^{\rm tot}$ across all sampling results, including those with σ = 0.1, 0.2, 0.5, 1.0, 1.5, 2.0 and 5.0, totaling 7000 samples, is presented.

B. Calculation results from experimental covariance matrix

In recent years, with the growing emphasis on covariance data in experiments and evaluations, more experiments have started reporting covariance data. The experimental data utilized in this work includes the reported covariance matrix [39, 40]. We can also utilize the reported covariance matrix from the experiment to generate perturbed PFNS using the aforementioned sampling method. The specific method is consistent with that described in Sec. II, with the only modification being the replacement of the covariance matrix generation part. We performed 600 samplings using the covariance data provided by the experiment and calculated the $\delta k_{\rm eff}^{\rm tot}$ values based on each perturbed PFNS. The distribution of $\delta k_{\rm eff}^{\rm tot}$ calculated using the PFNS sampled based on the experimental covariance matrix is presented in Fig. 6. This distribution shows a relatively higher probability at lower $\delta k_{\rm eff}^{\rm tot}$ values, which is beneficial for achieving faster convergence to the optimal value of $\delta k_{\rm eff}^{\rm tot}$. The optimal PFNS obtained through this sampling method, utilizing the covariance matrix is directly derived from the experiment, yields a $\delta k_{\rm eff}^{\rm tot}$ of 0.00208, which is slightly better than the previous results.

C. Discussion

We have generated covariance matrices for differential data using two distinct methods. One involves constructing a correlation matrix and combining it with experimental uncertainty information, henceforth referred to as Method 1. The other directly utilizes the covariance information provided by the experiment, henceforth referred to as Method 2. We perturbed the experimental data near its error range through random sampling and used the perturbed PFNS for transport calculations to conduct integral validation, thereby achieving the optimization of the differential PFNS.

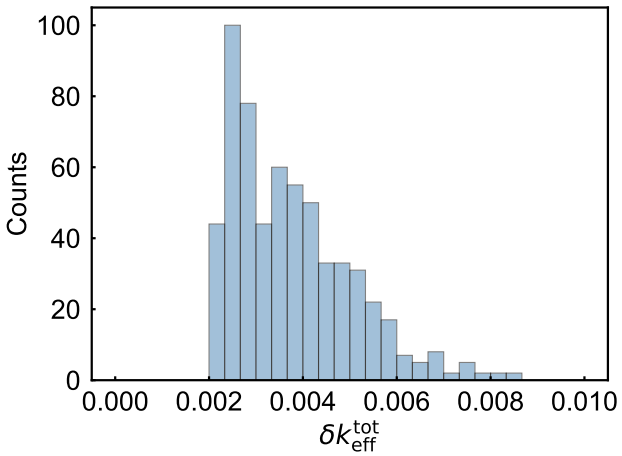

Fig. 6. The distribution of $\delta k_{\rm eff}^{\rm tot}$ calculated using the perturbed PFNS sampled from the experimental covariance matrix.

TABLE 1. A comparison between the optimal $\delta k_{\rm eff}^{\rm tot}$ values obtained through sampling using two methods for generating covariance matrices, and the $\delta k_{\rm eff}^{\rm tot}$ values calculated based on ENDF/B-VIII.0. Method 1 represents sampling based on the covariance matrix generated from the assumed correlation matrix and experimental uncertainties to obtain perturbed PFNS. Method 2 represents sampling based on the covariance matrix provided by the experiment to obtain perturbed PFNS.

source of PFNS	Method 1	Method 2	ENDF/B-VIII.0
$\delta k_{\rm eff}^{\rm tot}$	0.00210	0.00208	0.00299

Based on the results presented in Fig. 5 and Fig. 6, the distributions of $\delta k_{\rm eff}^{\rm tot}$ produced by the perturbed PFNS obtained through both methods exhibit a rapid decrease at low $\delta k_{\rm eff}^{\rm tot}$ values. The optimal PFNS values converged by the two methods are not significantly different. We have summarized the results in Table 1, which demonstrates that the optimized PFNS obtained through our random sampling method performs better in integral experiments compared to the PFNS provided by ENDF/B-VIII.0. Furthermore, Figs. 5 and 6 show that at the left end of the $\delta k_{\rm eff}^{\rm tot}$ distribution, it converges to a value near 0.002, rather than 0. This implies that merely adjusting the PFNS may not suffice to obtain a $k_{\rm eff}$ calculation value that is completely identical to the benchmark. However, we can still obtain a relatively better PFNS through this method.

Although both Method 1 and Method 2 can optimize the PFNS to approach an optimal value, differences in the covariance matrix lead to varying convergence speeds of the data near this optimal value. We can describe the distribution characteristics near low $\delta k_{\rm eff}^{\rm tot}$ by comparing the ratios of the

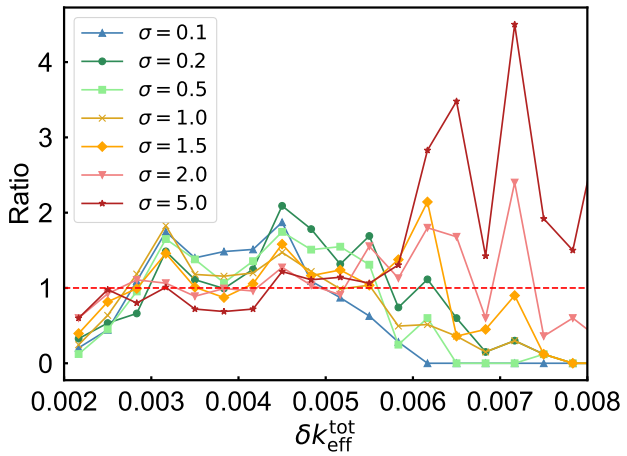

Fig. 7. (Color Online) The ratio depicted represents the comparison between the normalized distribution of $\delta k_{\rm eff}^{\rm tot}$ obtained under varying σ values using Method 1, and the normalized distribution of $\delta k_{\rm eff}^{\rm tot}$ calculated through covariance sampling derived from experimental data, denoted as Method 2. The red horizontal dashed line indicates a ratio of 1.

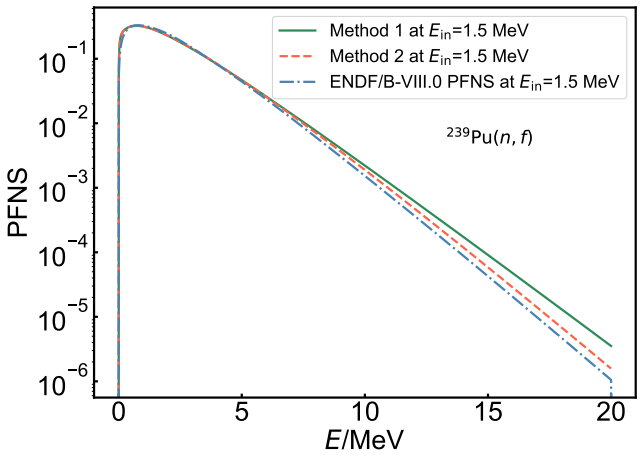

Fig. 8. (Color Online) A comparison of the optimized PFNS of ^{239}Pu(n, f) results obtained using Methods 1 and 2 with ENDF/B-VIII.0, illustrated using an incident energy of 1.5 MeV as a representative example.

distributions obtained from Method 1 and Method 2. Specifically, we use the distribution generated by Method 2 as the standard and compare the distribution histograms of $\delta k_{\rm eff}^{\rm tot}$ under different σ values in Method 1 with Fig. 6 by calculating their ratios. Specifically, after normalizing Fig. 3, Fig. 4(a), (b), (c), (d), (e) and (f) respectively, we calculated the ratio with the normalized histogram of Fig. 6 for each bin within the range of $\delta k_{\rm eff}^{\rm tot} = 0.002 \sim 0.008$ to obtain Fig. 7. The horizontal coordinates of the points in Fig. 7 represent the center values of the bins.

Fig. 7 illustrates that near the left end of the $\delta k_{\rm eff}^{\rm tot}$ distribution, the ratio of the distribution of $\delta k_{\rm eff}^{\rm tot}$ obtained from all samples in Method 1 to the distribution derived from Method 2 is less than one. This suggests that the covariance provided by the experimental data itself is more suitable for sampling to obtain the optimal PFNS. However, it should be noted that in cases where experimental covariance data are missing, Method 1, which constructs a correlation matrix combined with experimental uncertainty information to generate a covariance matrix for sampling, can also effectively approximate the optimal value. Although, compared to Method 2, it exhibits relatively lower efficiency near the optimal value. This observation aligns with the results presented in Table 1, demonstrating that Method 2 can achieve a better PFNS with fewer sampling instances.

Fig. 8 presents a comparison of the optimized PFNS results obtained using Methods 1 and 2 with ENDF/B-VIII.0, using an incident energy of 1.5 MeV as an example. It can be observed that the optimized PFNS shows slight variations from ENDF/B-VIII.0, and these variations contribute to the optimization of the integral experiment for calculating $k_{\rm eff}$. As can also be seen from Fig. 8, the method of utilizing integral experiments to constrain differential experiments demonstrates effective adjustment of PFNS, and due to the normalization of the spectrum, there is inevitably an interplay between the low-count and high-count parts of the final energy spectrum, and the distribution in the low-count region will be modulated by slight variations in the high-count region. From the results, the adjusted PFNS performs better in calculating criticality benchmarks. Consequently, we believe that the adjustment to the PFNS is beneficial for the entire spectrum, as it aligns well with both microscopic and integral experiments.

IV. SUMMARY AND PROSPECTS

In summary, we have introduced a method that utilizes integral criticality benchmark experiments to constrain the data of differential quantity, specifically the PFNS. By constructing a correlation matrix and combining it with experimental error data provided by experiments, we perturbed the measured central values. Subsequently, the perturbed PFNS was used as input data for transport simulations. The quality of the perturbed PFNS is evaluated by comparing the deviation between the calculated $k_{\rm eff}$ and the benchmark value of the criticality assemblies. Through extensive sampling, a set of optimal PFNS is obtained. In addition, this work examines the sampling method based on the covariance matrix derived from differential experiments. The results indicate that sampling utilizing the covariance matrix directly provided by experiments yields a higher probability of obtaining results close to the optimal value, thereby facilitating the achievement of better PFNS with fewer sampling instances. Notably, in terms of the optimal value, the method of generating a covariance matrix using an assumed correlation matrix is very close to the method utilizing the experimentally provided covariance matrix. This indicates that for data lacking an experimentally provided covariance matrix, our method can still be utilized to obtain relatively optimized PFNS through a finite number of sampling iterations.

It is also important to note that the optimal $\delta k_{\rm eff}^{\rm tot}$ we ob-

tained is not identically equal to 0,but rather a small value close to 0, specifically approximately 0.002. Furthermore, based on the distribution of $\delta k_{\rm eff}^{\rm tot}$ obtained from the sampling iteration and the observed decreasing trend at low $\delta k_{\rm eff}^{\rm tot}$, it can be inferred that merely adjusting the PFNS of ^{239}Pu is insufficient to make the $k_{\rm eff}$ value calculated from transport calculations completely identical to the benchmark value. This is due to the existence of other microscopic quantities that affect $k_{\rm eff}$, such as the cross-sections and the prompt neutron multiplicities of the neutron induced reaction of ^{239}Pu. This work further suggests that mutual constraints between multiple physical quantities can be achieved through criticality benchmark experiments. Moreover, this method, due to the added constraints from integral data, is beneficial for evaluating differential quantities that lack experimental data. Additionally, it facilitates the achievement of consistency between microscopic and macroscopic experimental data.

[1] J.C. Pei, W. Nazarewicz, J.A. Sheikh et al., Fission Barriers of Compound Superheavy Nuclei. Phys. Rev. Lett. **102**, 192501 (2009). https://doi.org/10.1103/PhysRevLett.102.192501

[2] W. Younes, D.M. Gogny, J. Berger, A Microscopic Theory of Fission Dynamics Based on the Generator Coordinate Method. *Lecture Notes in Physics* (2019) https://doi.org/10.1007/978-3-030-04424-4

[3] X.M. Shi, G.L. Wang, K.J. Luo et al., Geant4 development for actinides photofission simulation. Nucl. Instrum. Methods Phys. Res. A **1062**, 169222 (2024). https://doi.org/10.1016/j.nima.2024.169222.

[4] G.L. Wang, H.Y. Lan, X.M. Shi et al., A general framework for describing photofission observables of actinides at an average excitation energy below 30 MeV. Chin. Phys. C **46**, 084102 (2022). https://dx.doi.org/10.1088/1674-1137/ac6abc

[5] Y. Su, Z.Y. Li, L.L. Liu et al., Sensitivity impacts owing to the variations in the type of zero-range pairing forces on the fission properties using the density functional theory. Nucl. Sci. Tech. **35**, 62 (2024). https://doi.org/10.1007/s41365-024-01422-4

[6] N. Schunck, D. Regnier, Theory of nuclear fission. Prog. Part. Nucl. Phys. **125**, 103963 (2022). https://doi.org/10.1016/j.ppnp.2022.103963

[7] X.J. Sun, C.G. Yu, N. W. et al., Pre-neutron-emission mass distributions for reaction ^{238}U(n,f) up to 60 MeV. Chin. Phys. C **39**, 014102 (2015). https://doi.org/10.1088/1674-1137/39/1/014102

[8] X.L. Yang, C.L. Lan, Y.B. Nie et al., Cumulative fission yield measurements with 14.7 MeV neutrons on ^{238}U. Chin. Phys. C **47**, 024001 (2023). https://doi.org/10.1088/1674-1137/aca1ab

[9] C. Bhatia, B.F. Fallin, M.E. Gooden et al., Exploratory study of fission product yields of neutron-induced fission of ^{235}U,^{238} U, and ^{239}Pu at 8.9 MeV. Phys. Rev. C **91**, 064604 (2015). https://doi.org/10.1103/PhysRevC.91.064604

[10] A. Bulgac, S. Jin, I. Stetcu, Nuclear Fission Dynamics: Past, Present, Needs, and Future. Frontiers in Physics **8**(2020). https://doi.org/10.3389/fphy.2020.00063

[11] B. Liu, X. Zhang, F. Liu et al., The electron accelerator driven sub-critical system. Nucl. Eng. Des. **386**, 111567 (2022). https://doi.org/10.1016/j.nucengdes.2021.111567

[12] Y. Peneliau, O. Litaize, P. Archier et al., ^{239}Pu Prompt Fission Neutron Spectra Impact on a Set of Criticality and Experimental Reactor Benchmarks. Nucl. Data Sheets **118**, 459–462 (2014). https://doi.org/10.1016/j.nds.2014.04.106

[13] D. Neudecker, T. Taddeucci, R. Haight et al., The Need for Precise and Well-documented Experimental Data on Prompt Fission Neutron Spectra from Neutron-induced Fission of ^{2}39Pu. Nucl. Data Sheets **131**, 289–318 (2016). https://doi.org/10.1016/j.nds.2015.12.005

[14] X. Zou, L. Cao, Q. Teng et al., Uncertainty propagation of prompt fission neutron spectrum for physics analysis of fast and thermal reactors. Prog. Nucl. Energy **144**, 104077 (2022). https://doi.org/10.1016/j.pnucene.2021.104077

[15] T. Ethvignot, M. Devlin, R. Drosg et al., Prompt-fission-neutron average energy for ^{238}U(n,f) from threshold to 200 MeV. Phys. Lett. B **575**, 221–228 (2003). https://doi.org/10.1016/j.physletb.2003.09.048

[16] P. Staples, J. Egan, G. Kegel et al., Prompt fission neutron energy spectra induced by fast neutrons. Nucl. Phys. A **591**, 41–60 (1995). https://doi.org/10.1016/0375-9474(95)00119-L

[17] P. Talou, B. Becker, T. Kawano et al., Advanced Monte Carlo modeling of prompt fission neutrons for thermal and fast neutron-induced fission reactions on ^{239}Pu. Phys. Rev. C **83**, 064612 (2011). https://doi.org/10.1103/PhysRevC.83.064612

[18] A. Chatillon, G. Bélier, T. Granier et al., Measurement of prompt neutron spectra from the ^{239}Pu(n,f) fission reaction for incident neutron energies from 1 to 200 MeV. Phys. Rev. C **89**, 014611 (2014). https://doi.org/10.1103/PhysRevC.89.014611

[19] J. Lestone, E. Shores, Uranium and Plutonium Average Prompt-fission Neutron Energy Spectra (PFNS) from the Analysis of NTS NUEX Data. Nucl. Data Sheets **119**, 213–216 (2014). https://doi.org/10.1016/j.nds.2014.08.059

[20] P. Marini, J. Taieb, B. Laurent et al., Prompt-fission-neutron spectra in the ^{239}Pu$(n,\ f)$ reaction. Phys. Rev. C **101**, 044614 (2020). https://doi.org/10.1103/PhysRevC.101.044614

[21] J. Terrell, Fission Neutron Spectra and Nuclear Temperatures. Phys. Rev. **113**, 527–541 (1959). https://doi.org/10.1103/PhysRev.113.527

[22] B.E. Watt, Energy Spectrum of Neutrons from Thermal Fission of ^{235}U. Phys. Rev. **87**, 1037–1041 (1952). https://doi.org/10.1103/PhysRev.87.1037

[23] D.G. Madland, J.R. Nix, New Calculation of Prompt Fission Neutron Spectra and Average Prompt Neutron Multiplicities. Nucl. Sci. Eng. **81**, 213–271 (1982). https://doi.org/10.13182/NSE82-5

[24] Z.G. Ge, R.R. Xu, H.C. Wu et al., CENDL-3.2: The new version of Chinese general purpose evaluated nuclear data library. EPJ Web Conf. **239**, 09001 (2020). https://doi.org/10.1051/epjconf/202023909001

[25] D. Brown, M. Chadwick, R. Capote et al., ENDF/B-VIII.0: The 8th Major Release of the Nuclear Reaction Data Library with CIELO-project Cross Sections, New Standards and Thermal Scattering Data. Nucl. Data Sheets **148**, 1–142 (2018). https://doi.org/10.1016/j.nds.2018.02.001

[26] O. Iwamoto, N. Iwamoto, S. Kunieda et al., Japanese evaluated nuclear data library version 5: JENDL-5. J. Nucl. Sci. Technol. **60**, 1–60 (2023).

https://doi.org/10.1080/00223131.2022.2141903
[27] A.J.M. Plompen, The joint evaluated fission and fusion nuclear data library, JEFF-3.3. Eur. Phys. J. A **56**, 181 (2020). https://doi.org/10.1140/epja/s10050-020-00141-9
[28] P. Talou, T. Kawano, M.B. Chadwick et al., Uncertainties in nuclear fission data. J. Phys. G: Nucl. Part. Phys. **42**, 034025 (2015). https://doi.org/10.1088/0954-3899/42/3/034025
[29] G. Palmiotti, M. Salvatores, G. Aliberti et al., Combined Use of Integral Experiments and Covariance Data. Nucl. Data Sheets **118**, 596–636 (2014). https://doi.org/10.1016/j.nds.2014.04.145
[30] D. Neudecker, M. Grosskopf, M. Herman et al., Enhancing nuclear data validation analysis by using machine learning. Nucl. Data Sheets **167**, 36–60 (2020). https://doi.org/10.1016/j.nds.2020.07.002
[31] I. Kodeli, A. Trkov, R. Capote et al., Evaluation and use of the prompt fission neutron spectrum and spectra covariance matrices in criticality and shielding. Nucl. Instrum. Methods Phys. Res. A **610**, 540–552 (2009). https://doi.org/10.1016/j.nima.2009.08.076
[32] R. Capote, Y.J. Chen, F.J. Hambsch et al., Prompt Fission Neutron Spectra of Actinides. Nucl. Data Sheets **131**, 1–106 (2016). https://doi.org/10.1016/j.nds.2015.12.002
[33] D. Neudecker, R. Capote, H. Leeb, Impact of model defect and experimental uncertainties on evaluated output. Nucl. Instrum. Methods Phys. Res. A **723**, 163–172 (2013). https://doi.org/10.1016/j.nima.2013.05.005
[34] R. Capote, D. Smith, A. Trkov, Nuclear data evaluation methodology including estimates of covariances. EPJ Web Conf. **8**, 04001 (2010). https://doi.org/10.1051/epjconf/20100804001
[35] D. Neudecker, P. Talou, T. Taddeucci et al., Preliminary Evaluation and Uncertainty Quantification of the Prompt Fission Neutron Spectrum of ^{239}Pu. Nucl. Data Sheets **123**, 146–152 (2015). https://doi.org/10.1016/j.nds.2014.12.026
[36] Y.Y. Ding, Y.B. Nie, Y. Zhang et al., Benchmark experiment on slab ^{238}U with D-T neutrons for validation of evaluated nuclear data. Nucl. Sci. Tech. **35**, 29 (2024) https://doi.org/10.1007/s41365-024-01386-5
[37] Q. Zhao, Y.B. Nie, Y.Y. Ding et al., Measurement and simulation of the leakage neutron spectra from Fe spheres bombarded with 14 MeV neutrons. Nucl. Sci. Tech. **34**, 182 (2023). https://doi.org/10.1007/s41365-023-01329-6
[38] A. Trkov, R. Capote, V. Pronyaev, Current Issues in Nuclear Data Evaluation Methodology: ^{235}U Prompt Fission Neutron Spectra and Multiplicity for Thermal Neutrons. Nucl. Data Sheets **123**, 8–15 (2015). https://doi.org/10.1016/j.nds.2014.12.003
[39] K.J. Kelly, M. Devlin, J.M. O'Donnell et al., Measurement of the $^{239}\mathrm{Pu}(n,f)$ prompt fission neutron spectrum from 10 keV to 10 MeV induced by neutrons of energy 1–20 MeV. Phys. Rev. C **102**, 034615 (2020). https://doi.org/10.1103/PhysRevC.102.034615
[40] K.J. Kelly, J.M. O'Donnell, M. Devlin, The Covariance of PFNS Results from the Chi-Nu Experiment. EPJ Web Conf. **281**, 00026 (2023). https://doi.org/10.1051/epjconf/202328100026
[41] K.J. Kelly, P. Marini, J. Taieb et al., Comparison of Results from Recent NNSA and CEA Measurements of the $^{239}\mathrm{Pu}(n,f)$ Prompt Fission Neutron Spectrum. Nucl. Data Sheets **173**, 42–53 (2021). https://doi.org/10.1016/j.nds.2021.04.003
[42] K.J. Kelly, J.M. O'Donnell, D. Neudecker et al., The analysis of shape data including normalization and the impact on prompt fission neutron spectrum measurements. Nucl. Instrum. Methods Phys. Res., Sect. A **943**, 162449 (2019). https://doi.org/10.1016/j.nima.2019.162449
[43] L. Deng, G. Li, B.Y. Zhang et al., JMCT Monte Carlo Code with Capability of Integrating Nuclear System Feedback, in *Proceedings of the 2018 2nd International Conference on Applied Mathematics, Modelling and Statistics Application (AMMSA 2018)*, pp. 48-54, (2018), https://doi.org/10.2991/ammsa-18.2018.10.
[44] L. Deng, Z.H. Hu, R. Li et al., The coupled neutron transport calculation of Monte Carlo multi-group and continuous cross section. Ann. Nucl. Energy **127**, 433–436 (2019). https://doi.org/10.1016/j.anucene.2018.12.032
[45] L. Deng, G. Li, B.Y. Zhang et al., A high fidelity general purpose 3-D Monte Carlo particle transport program JMCT3.0. Nucl. Sci. Tech. **33**, 108 (2022). https://doi.org/10.1007/s41365-022-01092-0
[46] R. Macfarlane, D.W. Muir, R.M. Boicourt et al., The NJOY Nuclear Data Processing System, Version 2016. (2017). https://doi.org/10.2172/1338791
[47] R.D. Mosteller, F.B. Brown, B.C. Kiedrowski, An expanded criticality validation suite for MCNP. (2011). https://www.osti.gov/biblio/1083139
[48] N.E. Agency, ICSBEP Handbook 2019. (2019). https://doi.org/10.1787/e2703cd5-en
[49] K. Fan, Y.P. Yin, L.L. Song et al., Cross-Evaluation of the PU-MET-FAST criticality benchmark experiments in ICSBEP handbook (by the end of 2022). Nucl. Eng. Des. **415**, 112693 (2023). https://doi.org/10.1016/j.nucengdes.2023.112693
[50] https://github.com/mit-crpg/benchmarks/tree/master/icsbep